Mechanistic Investigation of Iridium-Catalyzed Hydrovinylation of Olefins

Jonas Oxgaard,[†] Gaurav Bhalla,[‡] Roy A. Periana,[‡] and William A. Goddard, III*,[†]

Materials and Process Simulation Center, Beckman Institute, Division of Chemistry and Chemical Engineering, California Institute of Technology, Pasadena, California 91125, and Loker Hydrocarbon Research Institute, Department of Chemistry, University of Southern California, Los Angeles, California 90089

Received October 16, 2005

C_2H_3-Ir(III)(acac-*O*,*O*)$_2$(Py) dimerizes olefins through a C−H activation mechanism. The starting catalyst first isomerizes to the cis conformer through a dissociative process, where pyridine is lost, and then adds the olefin substrate to the cis conformer. [1,2]-Insertion of the vinyl moiety into the coordinating olefin generates a Ir−CH_2−CH_2−CH═CH_2 complex, which then isomerizes to an Ir(η^3-allyl) complex through a series of β-hydride transfer reactions. The η^3-allyl complex is significantly more stable than any other part of the surface and is expected to be the resting state of the catalyst. Addition of a second olefin to the η^3-allyl complex leads to an Ir−(CH_2−CH═CH−CH_3) complex with a coordinating olefin, which can transfer a hydrogen to the product, 2-butene, via a C−H activation transition state. This transition step is the rate-determining step, with a calculated $\Delta H^{\ddagger} = 31.6$ kcal/mol and $\Delta G^{\ddagger} = 32.1$ kcal/mol. Other pathways were found to have reasonable barriers, but are not competitive due to very facile barriers leading to the η^3-allyl complex. From the allyl complex, neither 1-butene or butadiene are feasible products. The presence of 1-butene in the product mixture is attributed to isomerization of 2-butene; that is, it is not a kinetic product.

1. Introduction

Carbon−carbon bond-forming reactions are among the most important types of bond constructions in organic chemistry. One potentially important class of such reactions is the hydrovinylation of olefins, which forms the basis of the Dimersol technology and the Shell higher olefin process (SHOP).[1] These processes have been a topic of reviews and have been extended to other heterodimerization and asymmetric catalyses.[2] Common metal choices for hydrovinylation catalysts includes Rh,[3] Ru,[4] Pd,[5] and Ni.[6] The generally accepted mechanism for hydrovinylation involves a Cossee−Arlman-type migratory insertion of olefin into a metal hydride intermediate, which subsequently inserts into a second olefin to generate a metal-butenyl intermediate (see Figure 1). β-Hydride elimination yields the product, while addition of a new olefin closes the cycle.[7] Other mechanisms involving metallacyclopentane intermediates have also been postulated.[8] Only a related iridium complex, Tp*Ir(C_2H_4)$_2$, has been shown to form a hydrido-allyl derivative via the insertion of ethylene into the Ir−vinyl stoichiometrically, produced by the CH activation of ethylene.[9]

Recently, we reported that the O-ligated complex C_2H_3-Ir(III)(acac-*O*,*O*)$_2$(Py) (acac-*O*,*O* = κ^2-*O*,*O*-acetylacetonate, Py = pyridine), **Vinyl-Ir-Py** [where −Ir− is understood to be Ir(III)(acac-*O*,*O*)$_2$ throughout this paper], inserts olefins and catalyzes the dimerization of olefins via a C−H activation pathway.[10] Heating **Vinyl-Ir-Py** in hexaflourobenzene with ethylene at 180 °C results in the formation of 1-butene and *cis*- and *trans*-2-butene in a 1:2:1 ratio (TN = 32, TOF $\approx 10 \times 10^{-3}$ s^{-1}). Similarly, carrying out the reaction with propylene results in the formation of various hexene isomers as observed by GC/MS analysis. Similar results are obtained when **CH_3-Ir-Py** is used as a catalyst. This is the first system to carry out this reaction in a catalytic fashion.

We have previously reported preliminary theoretical calculations on this mechanism, where we concluded that the mech-

* To whom correspondence should be addressed. E-mail: wag@wag.caltech.edu.

[†] California Institute of Technology.

[‡] University of Southern California.

(1) (a) Wilke, G.; Bogdanovic, B.; Hardt, P.; Heimbach, P.; Keim, W.; Kroner, M.; Oberkirch, W.; Tanaka, K.; Steinrucke, E.; Walter, D.; Zimmermann, H. *Angew. Chem., Int. Ed. Engl.* **1966**, *5*, 151. (b) Chauvin, Y., Olivier, H. In *Applied Homogeneous Catalysis with Organometallic Compound*; Cornils, B., Herrmann, W. A., Eds.; VCH: New York, 1996; Vol. 1, p 258. (c) Keim, W. *Angew. Chem., Int. Ed. Engl.* **1990**, *29*, 235.

(2) (a) Ittel, S. D.; Johnson, L. K.; Brookhart, M. *Chem. Rev.* **2000**, *100*, 1169. (b) RajanBabu, T. V. *Chem. Rev.* **2003**, *103*, 2845. (c) Pillai, S. M.; Ravindranathan, M.; Sivaram, S. *Chem. Rev.* **1986**, *86*, 353.

(3) (a) Alderson, T.; Jenner E. T.; Lindsey, R. V. J. *J. Am. Chem. Soc.* **1965**, *87*, 5638 (b) Brookhart M.; Sabo-Etienne, S. *J. Am. Chem. Soc.* **1991**, *113*, 2777. (c) Brookhart, M.; Hauptman, E. *J. Am. Chem. Soc.* **1992**, *114*, 4437. (d) Hauptman, E.; Etienne, S. S.; White, P. S.; Brookhart, M.; Garner, J. M.; Fagan, P. J.; Calabrese, J. C. *J. Am. Chem. Soc.* **1994**, *116*, 8038.

(4) (a) McKinney, R. J.; Colton, M. C. *Organometallics* **1986**, *5*, 1080. (b) Pertici, P.; Ballantini, V.; Salvadori, P.; Bennett, M. A. *Organometallics* **1995**, *14*, 2565.

(5) (a) Rix, F. C.; Brookhart, M. *J. Am. Chem. Soc.* **1995**, *117*, 1137. (b) DiRenzo, G. M.; White, P. S.; Brookhart, M. *J. Am. Chem. Soc.* **1996**, *118*, 6225. (c) Shultz, L. H.; Brookhart, M. *Organometallics* **2001**, 20, 3975.

(6) (a) Hicks, F. A.; Brookhart, M. *Organometallics* **2001**, *20*, 3217 (b) Liu, W.; Malinoski, J. M.; Brookhart, M. *Organometallics* **2002**, *21*, 2836.

(7) (a) DiRenzo, M. G.; White, P. S.; Brookhart, M. *J. Am. Chem. Soc.* **1996**, *118*, 6225. (b) Hauptman, E.; Sabo-Etienne, S.; White, P. S.; Brookhart, M.; Garner, M. J.; Fagan, P. J.; Calabrese, J. C. *J. Am. Chem. Soc.* **1994**, *116*, 8038.

(8) (a) McLain, S. J.; Schrock, R. R.; *J. Am. Chem. Soc.* **1978**, *100*, 1315. (b) McLain, S. J.; Sancho, J.; Schrock, R. R. *J. Am. Chem. Soc.* **1978**, *102*, 1315. (c) Grubbs, R. H.; Miyashita, A. *J. Am. Chem. Soc.* **1978**, *100*, 1300.

(9) (a) Perez, P. J.; Poveda, M. L.; Carmona, E. *J. Chem. Soc., Chem. Commun.* **1992**, 8. (b) Alvarado, Y.; Boutry, O.; Gutierrez, E.; Monge, A.; Nicasio, M. C.; Poveda, M. L.; Perez, P. J.; Ruiz, C.; Bianchini, C.; Carmona, E. *Chem. Eur. J.* **1997**, *3*, 860.

(10) Bhalla, G.; Oxgaard, J.; Periana, R. A.; Goddard, W. A., III. *Organometallics* **2005**, *24*, 5499.

10.1021/om050890x CCC: $33.50
Publication on Web 02/24/2006

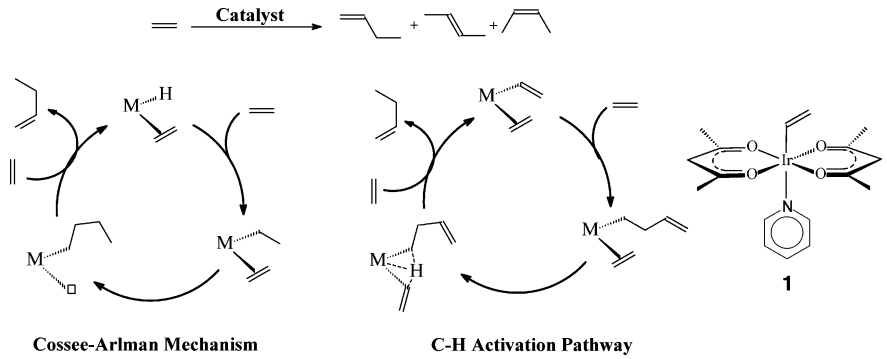

Figure 1. Left: Competing pathways for dimerization of ethylene. Right: Structure of **Vinyl-Ir-Py** (**1**).

anism is similar to the mechanism for hydroarylation.[11] The key step is a [1,2]-insertion into a complexed olefin, and product formation is realized through C−H activation. However, as the hydroarylation reaction is inhibited by the presence of excess olefin (benzene/ethene ratios > 0.2) while the hydrovinylation intrinsically has an "excess" of olefin, one cannot directly compare the mechanisms. Furthermore, the presence of multiple products indicates a significantly added complexity to the mechanism, the origin of which is not a priori clear.

In this publication we aim to present the complete computational results of the possible mechanisms for the hydrovinylation.

2. Computational Methodology

All calculations were performed using the hybrid DFT functional B3LYP as implemented by the Jaguar 5.5 and 6.0 program packages.[12] This DFT functional utilizes the Becke three-parameter functional[13] (B3) combined with the correlation functional of Lee, Yang, and Parr[14] (LYP) and is known to produce good descriptions of reaction profiles for transition metal containing compounds.[15,16] The metals were described by the Wadt and Hay[17] core-valence (relativistic) effective core potential (treating the valence electrons explicitly) using the LACVP basis set with the valence double-ζ contraction of the basis functions, LACVP**. All electrons were used for all other elements using a modified variant of Pople's[18] 6-31G** basis set, where the six d functions have been reduced to five.

Implicit solvent effects of the experimental benzene medium were calculated with the Poisson−Boltzmann (PBF) continuum approximation,[19] using the parameters $\epsilon = 2.284$ and $r_{solv} = 2.602$ Å. Due to the increased cost of optimizing systems in the solvated phase (increase in computation time by a factor of ∼4), solvation effects are calculated here as single-point solvation corrections to gas-phase geometries. Our previous work on the Ir(acac)$_2$ system has shown that the total energies, geometries, frequencies, and zero-point energies were also largely unchanged when the systems were optimized in the solvation phase.[11] Indeed, as these system are essentially nonpolar systems in a nonpolar solvent, the gas-phase enthalpies were within 5 kcal/mol of the solvent enthalpies.

All energies here are reported as $\Delta H(0\text{ K}) = \Delta E$ + zero-point energy correction + solvation correction. Relative energies on the $\Delta H(0\text{ K})$ surface are expected to be accurate to within 3 kcal/mol for stable intermediates and within 5 kcal/mol for transition structures.[20] Moreover, relative energies of isoelectronic species (such as regioisomers) are considerably more accurate, since the errors largely cancel.

Free energies were calculated as $\Delta G(473\text{ K}) = \Delta H(473\text{ K}) - T\Delta S(473\text{ K})$, where $\Delta H = \Delta E(\text{gas phase}) + \Delta E(\text{solvation correction}) + \text{ZPE} + \Delta H(\text{vib}) + 3kT\Delta(n)$. The last term, $3kT$, is a fixed value for the sum of the rotational and translational contributions to the enthalpy at 473 K, calculated to be 2.823944 kcal/mol. ΔS terms were calculated by summing the $\Delta S(\text{vib}) + \Delta S(\text{trans/rot}) + \Delta S(\text{conc})$. $\Delta S(\text{vib})$ is taken from the Jaguar gas-phase calculation at 473 K, while $\Delta S(\text{trans/rot})$ is given a fixed value of 30 cal/(mol K).

The use of $3kT$ and 30 cal/(mol K) for the $\Delta H(\text{trans/rot})$ and $\Delta S(\text{trans/rot})$ terms, respectively, was made to avoid the values obtained in the gas-phase calculations of thermodynamic properties. For a solvated reaction these gas-phase values are substantially inflated,[21] and accurate values most likely require a full dynamic simulation. As this is outside the scope of this paper, however, we elected to use a fixed value reflecting the experimental value for a pure liquid.

All geometries were optimized and evaluated for the correct number of imaginary frequencies through vibrational frequency calculations using the analytic Hessian. Zero imaginary frequencies corresponds to a local minimum, while one imaginary frequency corresponds to a transition structure. Although the singlet states are expected to be the lowest energy spin states, we also investigated higher spin states for select geometries and invariably found the singlet as the lowest energy state.

To reduce computational time, the methyl groups on the acac ligands were replaced with hydrogens. Control calculations show that relative energies of intermediates and transition structures change less than 0.1 kcal/mol when methyl groups are included.

3. Results

3.1. Cis/Trans Isomerization. The first step of the mechanism is the isomerization of the trans **Vinyl-Ir-Py** into the cis

(11) (a) Oxgaard, J.; Periana, R. A.; Goddard, W. A., III. *J. Am. Chem. Soc.* **2004**, *126*, 11658. (b) Oxgaard, J.; Muller, R. P.; Periana, R. A.; Goddard, W. A., III. *J. Am. Chem. Soc.* **2004**, *126*, 352.

(12) *Jaguar 5.5*; Schrodinger, Inc.: Portland, OR, 2000. *Jaguar 6.0*; Schrodinger, Inc.: Portland, OR, 2005.

(13) Becke, A. D. *J. Chem. Phys.* **1993**, *98*, 5648.

(14) Lee, C.; Yang, W.; Parr, R. G. *Phys. Rev. B* **1988**, *37*, 785.

(15) Baker, J.; Muir, M.; Andzelm, J.; Scheiner, A. In *Chemical Applications of Density-Functional Theory*; Laird, B. B., Ross, R. B., Ziegler, T., Eds.; ACS Symposium Series 629; American Chemical Society: Washington, DC, 1996.

(16) Niu, S.; Hall, B. M. *Chem. Rev.* **2000**, *100*, 353.

(17) (a) Hay, P. J.; Wadt, W. R. *J. Chem. Phys.* **1985**, *82*, 299. (b) Goddard, W. A., III. *Phys. Rev.* **1968**, *174*, 659. (c) Melius, C. F.; Olafson, B. O.; Goddard, W. A., III. *Chem. Phys. Lett.* **1974**, *28*, 457.

(18) (a) Hariharan, P. C.; Pople, J. A. *Chem. Phys. Lett.* **1972**, *16*, 217. (b) Francl, M. M.; Pietro, W. J.; Hehre, W. J.; Binkley, J. S.; Gordon, M. S.; DeFrees, D. J.; Pople, J. A. *J. Chem. Phys.* **1982**, *77*, 3654.

(19) (a) Tannor, D. J.; Marten, B.; Murphy, R.; Friesner, R. A.; Sitkoff, D.; Nicholls, A.; Ringnalda, M.; Goddard, W. A., III; Honig, B. *J. Am. Chem. Soc.* **1994**, *116*, 11875. (b) Marten, B.; Kim, K.; Cortis, C.; Friesner, R. A.; Murphy, R. B.; Ringnalda, M. N.; Sitkoff, D.; Honig, B. *J. Phys. Chem.* **1996**, *100*, 11775.

(20) Bhalla, G.; Liu, X. Y.; Oxgaard, J.; Goddard, W. A., III; Periana, R. A. *J. Am. Chem. Soc.* **2005**, *127*, 11372

(21) (a) Truong, T. N.; Truong, T. T.; Stefanovich, E. V. *J. Chem. Phys.* **1997**, *107*, 1881. (b) Cramer, C. J.; Thrular, D. G. *Chem. Rev.* **1999**, *99*, 2161.

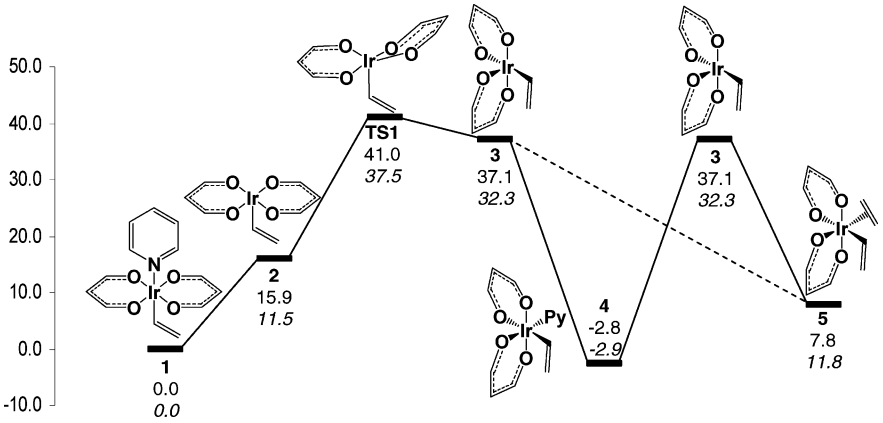

Figure 2. Calculated pathway for isomerization of catalyst precursor. Enthalpies and *free energies* in kcal/mol.

form. This isomerization was investigated in depth for the analogous Phenyl-Ir-L (L = H_2O, Py) catalyst (theoretically[11a] as well as experimentally[20]) and was found to isomerize through a dissociative unimolecular process.

Replacing the phenyl group with a vinyl group changes this mechanism very little. Calculations on the dissociative mechanism (Figure 2) show that **1** can easily dissociate pyridine to generate **2**, with a $\Delta H = 15.9$ kcal/mol. The five-coordinate **2** can then undergo a cis/trans isomerization (**TS1**) with a $\Delta H^{\ddagger} = 41.0$ kcal/mol (25.1 kcal/mol with respect to **2**). The isomerization occurs through movement of one of the four acac-ligand oxygens to a position trans to the vinyl group. **TS1** is a fairly late transition state, as observed in the O−Ir−O angle of 114.1°. This is a reflection of the Hammond postulate, as the result of the isomerization (the five-coordinate species **3**) is a high-energy species, 22.2 kcal/mol higher in energy than **2**. The high energy of **3** is caused by the distortion of aromatic stabilization in the acac rings due to trans influence from the vinyl carbon. This has been studied in more detail in a previous publication by this group.[11a.]

3 can coordinate to either pyridine (**4**, $\Delta H = -39.9$ kcal/mol) or ethene (**5**, $\Delta H = 29.3$ kcal/mol). As **4** is significantly more stable than **5**, this is expected to be the resting state of the catalyst. This has been confirmed experimentally for the phenyl analogue, where it was found that in the absence of an olefin **4** is formed quantitatively.[20] Under normal experimental conditions,[22] however, the concentration of ethene is significantly larger than the concentration of free pyridine, and it is thus very likely that the majority of **3** will go directly to **5**.

3.2. Olefin Insertion. Insertion of the vinyl group in **5** into the olefin (**TS2**, Figure 3) generates a metal-butene species (**6**), where the double bond is in the terminal position. **TS2** is a classic [1,2]-insertion transition state where an Ir−C and a C═C bond are broken while an Ir−C and a C−C bond are created simultaneously (see Figure 4). The activation energy of the insertion, 30.6 kcal/mol (22.8 kcal/mol with respect to **5**), is somewhat lower than the insertion activation energy for the phenyl analogue (34.0 and 24.5 kcal/mol, respectively).[11a] This is most likely due to the disruption of aromaticity in the phenyl transition state, which is not necessary in **TS2**. Consequently, the bond lengths of the breaking Ir−C and the forming C−C bonds are both shorter in **TS2** than in the phenyl analogue, by 0.06 and 0.04 Å, respectively.

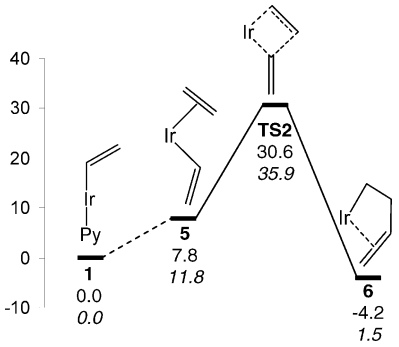

Figure 3. Calculated pathway for olefin insertion. Enthalpies and *free energies* in kcal/mol.

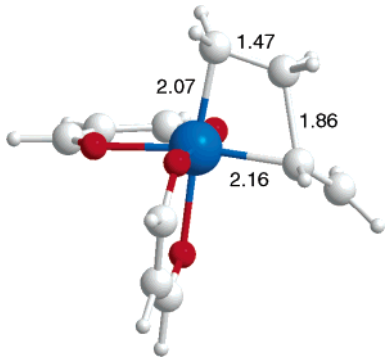

Figure 4. Geometry of **TS2**. Distances in Å.

The product of the insertion is the chelating complex **6**. The reaction is exothermic by 12.0 kcal/mol on the ΔH surface. The conversion of a double bond to two single bonds is expected to gain the system ~20 kcal/mol in energy, indicating that the coordination of the terminal olefin in **6** is less favorable than coordination of the ethene in **5**, most likely due to the strain caused by the relatively short tether. The analogue reaction in the arylation process is endothermic by 3.1 kcal/mol, reflecting the poor coordination of the tethered aryl unit to the metal center.

3.3. Generation of 1-Butene through C−H Activation. Rotation of the butene group can generate a coordinately unsaturated species (**7**), which enables complexation of a second olefin (**8**) (see Figure 5). The relative energy of **7** is 22.3 kcal/mol, 26.5 kcal/mol higher in energy than **6**. Coordination of the second olefin is exothermic by 29.4 kcal/mol, demonstrating the increased coordination energy due to the lack of strain. **8** is the lowest energy species on the ΔH surface, although the positive entropy term associated with the inclusion of a second olefin suggests that the conversion **6** → **8** is slightly endothermic on the ΔG surface.

(22) (a) Matsumoto, T.; Taube, D. J.; Periana, R. A.; Taube, H.; Yoshida, H. *J. Am. Chem. Soc.* **2000**, *122*, 7414. (b) Matsumoto, T.; Periana, R. A.; Taube, D. J.; Yoshida, H. *J. Mol. Catal. A* **2002**, 1. (c) Matsumoto, T.; Yoshida, H. *Catal. Lett.* **2001**, *72*, 107. (d) Periana, R. A.; Liu, Y. X.; Bhalla, G. *Chem. Commun.* **2002**, 3000.

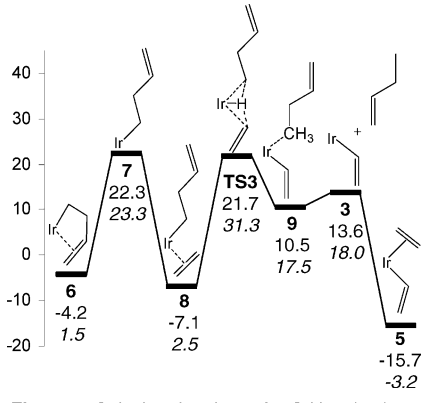

Figure 5. Calculated pathway for C−H activation leading to 1-butene. Enthalpies and *free energies* in kcal/mol.

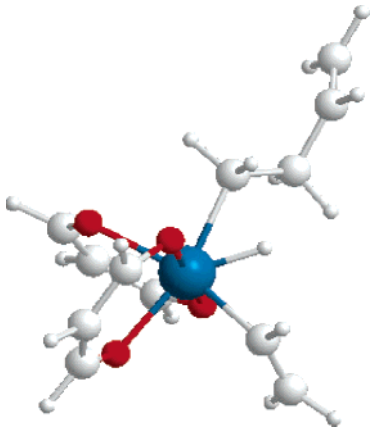

Figure 6. Geometry of **TS3**. Distances in Å.

The olefin in **8** can transfer a hydrogen to the metal-butenyl species through a mechanism previously characterized as oxidative hydrogen migration (OHM) (**TS3**).[11] This is a concerted mechanism with a transition state similar to an oxidative addition intermediate, featuring a fully formed bond between the iridium and the migrating hydrogen (1.56 Å, see Figure 6). The distances between the hydrogen and the two carbons are 1.93 and 1.70 Å, indicative of partially formed bonds. The $\Delta H^{\ddagger}$ of **TS3** is calculated to be 28.9 kcal/mol, similar in magnitude to $\Delta H^{\ddagger}$(**TS2**) at 30.6 kcal/mol. As was the case on previous occasions when an OHM style transition state was encountered,[11] no formally Ir^{V} intermediate could be isolated, with all attempts collapsing to either **8** or **9**.

TS3 yields **9**, an iridium vinyl complex with the product 1-butene weakly coordinating to the metal in an agostic fashion. Generation of **9** is endothermic by 17.6 kcal/mol, reflecting the loss of coordination energy in exchanging the olefin complexation for the much less favorable agostic interaction.

With the 1-butene only weakly coordinating, loss of ligand is uphill an additional 2.9 kcal/mol, leading to the coordinatively unsaturated complex **3**. Complexation of an a new ethene regenerates the catalyst and thus completes the catalytic cycle. Coordination of the ethene is exothermic by 29.3 kcal/mol, and the transformation **8** + ethene → **5** + 1-butene is exothermic by 8.6 kcal/mol, thus providing a driving force for the latter half of the catalytic cycle.

3.4. Generation of 2-Butene through C−H Activation. The mechanism above cannot be the complete mechanism, however, as indicated by the experimental observance of *cis*- and *trans*-2-butene. The product distribution is caused by isomerization of the metal-butene through a methyl η^3-allyl moiety (**13**), starting from intermediate **6** (Figure 7). Instead of coordinating an olefin to the iridium-butyl species, **6** undergoes a β-hydride transfer (BHT) (**TS4**, see Figure 8) to yield the metal-hydride butadiene species **10**. The barrier for the transfer is 17.4 kcal/mol, and the thermodynamics are moderately uphill, 4.2 kcal/mol. It is likely that an agostic intermediate exists prior to **TS4** where the coordinating olefin has rotated outward by ~60°, but no such intermediate could be located, via either regular optimization or IRC calculations from **TS4**. As can be seen for structure **12**, the energy of this intermediate would be very close

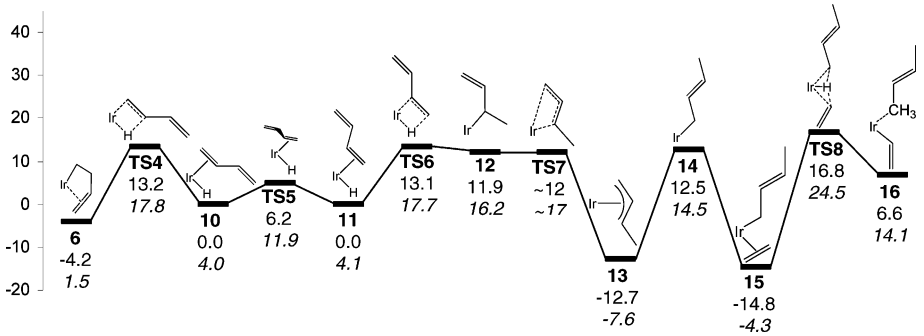

Figure 7. Calculated pathway for C−H activation leading to 2-butene. Enthalpies and *free energies* in kcal/mol.

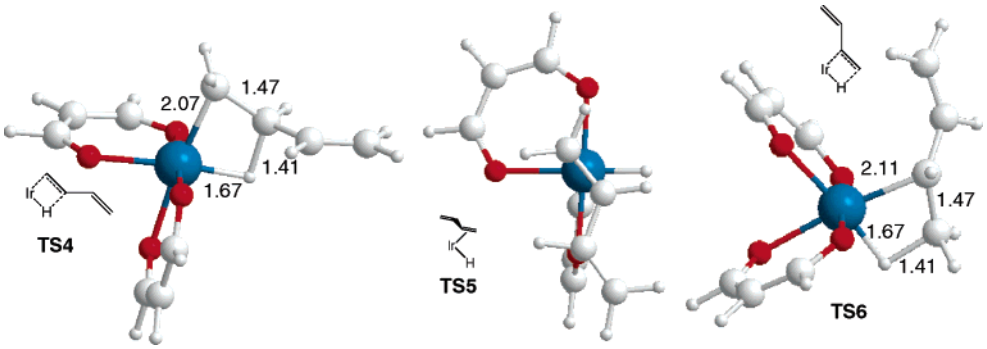

Figure 8. **TS4**, **TS5**, and **TS6**. Distances in Å.

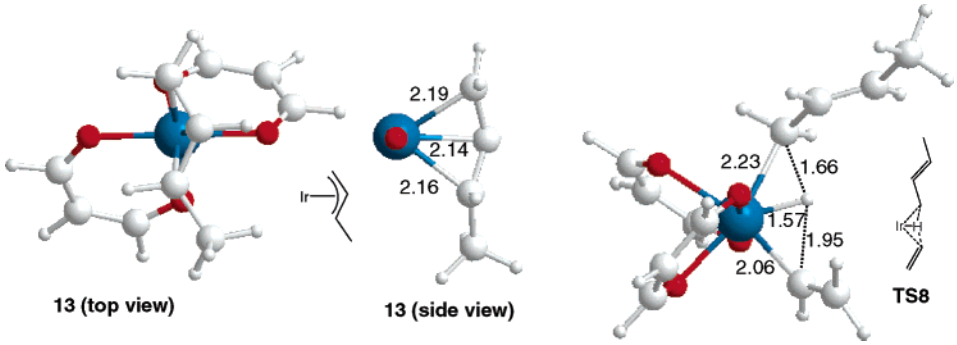

Figure 9. **13** (top and side view) and **TS8**. Distances in Å. Acac ligands in **13**, side view omitted for clarity.

to the energy of **TS4** and is not expected to add to the overall barrier. **TS4** is a traditional BHT transition state, with the four reacting atoms in a plane (φ(Ir−C−C−H) = 1.2°). The Ir−H distance is, at 1.67 Å, fairly short (the full Ir−H bond in **10** has a distance of 1.57 Å), while the C−H distance is a fairly long, 1.41 Å.

The butadiene moiety in **10** can easily rotate around the coordinating olefin, to generate the rotamer **11**. The energies of the two rotamers are identical (within the accuracy of the computational method), and the barrier for rotation (**TS5**) is calculated to be 6.2 kcal/mol. Technically the rotation process is a stepwise mechanism with two transitition states corresponding to rotations of the olefin of ±45° (TS), ±90° (intermediate), and ±135° (TS), but only the highest energy state is shown here.

From **11** a migratory insertion (**TS6**) occurs, with a barrier of 13.1 kcal/mol with respect to **11** and 17.3 kcal/mol with respect to **6**. Functionally, this insertion is a reverse BHT, and the transition state **TS6** is very similar to **TS4**, with identical Ir−H and C−H bond lengths. The product of **TS6** is **12**, a methyl σ-allyl complex where one of the hydrogens on the methyl group coordinates to the iridium in an agostic fashion. The calculated ΔH of **12** is 11.9 kcal/mol.

12 collapses easily into the methyl η^3-allyl complex **13** (see Figure 9). A transition state connecting **12** and **13** could not be located, as any deviation from the geometry of **12** immediately led to **13**. A similar result has previously been reported for Ir(η^3-allyl)$_3$ by John et al.,[23] where only the transition state but not the intermediate could be located. Furthermore, since **12** could be found only through an IRC calculation from **TS6**, it appears that the hypersurface is very flat in this region, obstructing a computational separation of intermediate and transition state. However, this also means that the energy of **TS7** should be very close to the energy of **12**, and while this might be the highest barrier between **6** and **13**, it is still significantly lower in energy than **TS2**.

13 is, like most metal η^3-allyls, a relatively stable complex. With a ΔH of −12.7 kcal/mol, the transformation of **12** → **13** is exothermic by 26.4 kcal/mol. This is somewhat more favorable than the ∼21 kcal/mol found by John et al. for the triallyl complex,[23] possibly due to the less electron donating character of the acac oxygens. The low energy of **13** establishes this as the new ground state of the system, which has some fairly drastic implications for the mechanism of this process. While the activation energy of **TS2** with respect to **1** is 30.6 kcal/mol, with respect to **13** it is 42.9 kcal/mol, effectively making this pathway energetically inaccessible. This is further discussed in section 4.

(23) John, K. D.; Michalczyk, R.; Hernandez, G.; Green, J. C.; Martin, R. L.; Baker, R. T.; Sattelberger, A. P. *Organometallics*, **2002**, *21*, 5757

Dissociation of the allyl ligand yields the five-coordinate σ-butenyl species **14**, with an energy of 12.8 kcal/mol. Again, no transition state connecting **13** to **14** could be found, as **14** easily collapsed back to **13**. Furthermore, as **14** has no agostic interactions, it is 0.6 kcal/mol higher in energy than **12**, even though the internal π-bond should confer some stability relative to the terminal π-bond in **12**.

The open site enables coordination of a second ethene, leading to complex **15**. Attempts at finding a concerted process for the transformation of **13** → **15** were unsuccessful, leading us to believe that even if such a process exists the energy should be similar to or higher than the dissociative process (i.e., through **14**). However, it is possible that the ethene intercepts the vacant site as it is being formed, thus driving the process forward. Like **8**, **15** is somewhat more stable than **13** on the ΔH surface but somewhat less stable on the ΔG surface due to a positive ΔS term.

From **15** C−H activation (**TS8**) forms the *trans*-2-butene product **16**, using a transition state very similar to **TS3**. The activation energy is 31.6 kcal/mol from **15**, suggesting that **TS8** is the rate-determining step in the catalytic cycle. This also suggests that **13** and/or **15** could be trapped, as they are the resting state for the catalyst.

From the agostic complex **16** *trans*-2-butene is exchanged for ethene in a fashion identical with the mechanism for generation of 1-butene, and is not shown.

It should also be mentioned that all structures above show the *trans*-butene or anti-allyl conformation. Control calculations of the *cis*-butene and syn-allyl species show that these transition states and intermediates react through the same mechanism, although consistently ∼2 kcal/mol higher in energy than the trans/anti pathway.

3.5. Cossee−Arlman Mechanism. The Cossee−Arlman mechanism is expected to initiate in the same fashion as the C−H activation pathway, i.e., cis/trans isomerization, coordination of olefin, and [1,2]-insertion to yield **6**. As the starting catalyst contains a vinyl moiety, the catalyst must produce 1 equiv of butadiene (**18**) before a metal-ethyl species is formed. This would initially follow the same mechanism as isomerization of the metal-butenyl species described in section 3.4 (i.e., **6** → **10**). From **10** the butadiene dissociates, leaving a five-coordinate Ir−H species (**17**) with a calculated ΔH of 30.2 kcal/mol. The Cossee−Arlman mechanism is summarized in Figure 10.

Coordination of a second ethene to replace the butadiene is exothermic by 33.5 kcal/mol, leading to complex **18**. The calculated ΔH is of the same magnitude as the olefin coordination in the cis/trans isomerization (**3** → **5**, ΔH = −29.3 kcal/mol), due to the similar electronic nature of iridium−hydride and iridium−vinyl bonds.

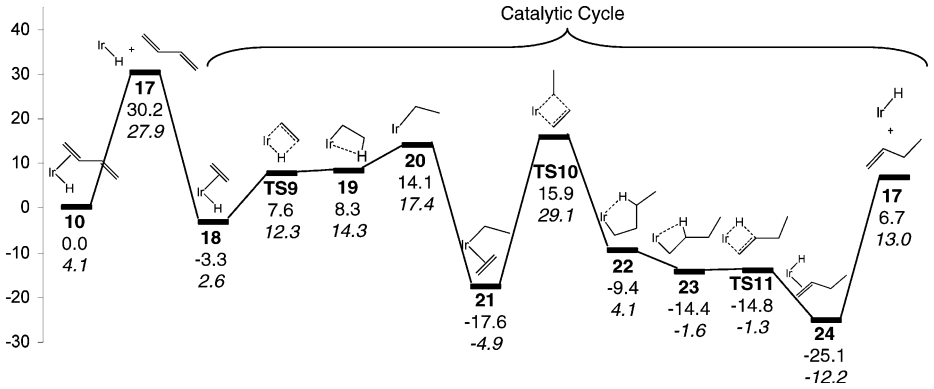

Figure 10. Calculated pathway for Cossee−Arlman mechanism leading to 1-butene. Enthalpies and *free energies* in kcal/mol.

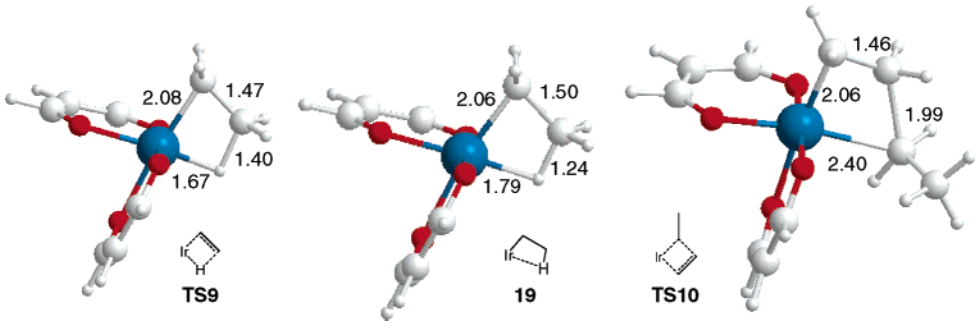

Figure 11. **TS9**, **19**, and **TS10**. Distances in Å.

A migratory insertion from **18** occurs through **TS9**, with a $\Delta H^{\ddagger} = 10.9$ kcal/mol. **TS9** is similar to other BHT-type transition states described above (see Figure 11) and leads to the agostic Ir-ethyl species **19**. Our calculations show that **19** is 0.7 kcal/mol *higher* in energy than **TS9**, most likely due to inaccuracies in the ZPE corrections. On the ΔE surface **19** is 0.5 kcal/mol lower in energy than **TS9** (in both the gas phase and solvent phase).

Rotation around the Ir−C bond in **19** leads to the five-coordinate species **20**, with a $\Delta H = 5.8$ kcal/mol. The open coordination site enables association of a new ethene, with a $\Delta H = -31.7$ kcal/mol (**21**). Similarly to **TS2**, [1,2]-insertion (**TS10**) into the ethene ligand couples the two carbons. The $\Delta H^{\ddagger}$ of **TS10** is calculated to be 33.5 kcal/mol, which is 10.7 kcal/mol higher in energy than the $\Delta H^{\ddagger}$ of **TS2**. This difference is most likely caused by the absence of accessible π-orbitals on the ethyl moiety, forcing the insertion into the localized sp^3-orbital on the migrating carbon. This is also reflected in the geometry of **TS10** (see Figure 11), which has considerably longer bond lengths to the migrating carbon as compared with **TS2**.

As there is no unsaturated bond in the insertion product (**22**), the lack of a possible olefin coordination makes the insertion endothermic by 8.2 kcal/mol. **22** features an agostic interaction between the iridium and one of the γ-hydrogens, formed as the C−C bond is closed. Exchanging this interaction for an agostic interaction with a β-hydrogen (**23**) is exothermic by 5 kcal/mol, possibly due to hyperconjugation in **23**. BHT of this hydrogen occurs through the transition state **TS11**, which has a negligible barrier of 0.5 kcal/mol, and leads to the iridium hydride species **24**. Investigations of possible γ-hydride eliminations from **22** did not lead to any feasible mechanisms, as scanning the breaking C−H bond showed barriers > 30 kcal/mol.

Dissociation of the terminal 1-butene ligand in **24** leads to the five-coordinate iridium hydride **17**, thus completing the catalytic cycle. As the 1-butene binds slightly stronger to the metal than butadiene, the dissociation is exothermic by 31.8 kcal/mol.

The mechanism for generation of 2-butene is expected to follow an isomerization pattern similar to that described for the C−H activation pathway and was not further investigated.

3.7. Reductive Coupling. Reductive coupling, as shown by Morokuma and co-workers,[24] was also investigated, but no stable Ir^{V} intermediate could be isolated. This is not surprising, as the presence of the OHM transition states **TS3** and **TS8** in lieu of regular oxidative addition intermediates indicates that other oxidative addition intermediates of similar nature would be inaccessible.

Scheme 1. Conceptual Reductive Coupling

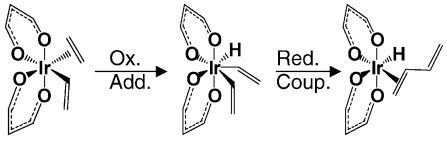

3.8. Free Energies. While the above sections feature discussions of the calculated ΔH values, we also calculated the free energy for each species. However, these energies are normally significantly less accurate than the ΔH energies, and as there are no experimentally determined ΔG values for these reactions, we cannot ascertain how accurate these results are.

Nevertheless, the calculated ΔG(473 K) values are included in the above diagrams, and it is clear that while the overall surface becomes higher in energy, barriers are generally of the same magnitude as the ΔH barriers. The notable exception to this, however, is the key transition of the Cossee−Arlman mechanism, which on the ΔH surface has a barrier of 34.4 kcal/mol, but on the ΔG surface is only 29.4 kcal/mol. This change

(24) Ananikov, V. P.; Musaev, D. G.; Morokuma, K. *J. Am. Chem. Soc.* **2002**, *124*, 2839.

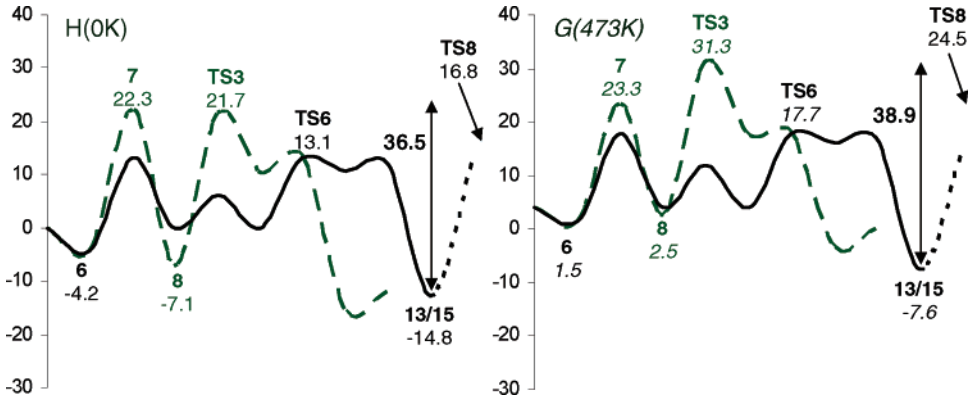

Figure 12. Comparisons of key steps for C−H activation pathways leading to 1-butene (green dashed line) and 2-butene (solid black line) (ΔH(0 K) left and ΔG(473 K) right). Note that steps after **13** are not included.

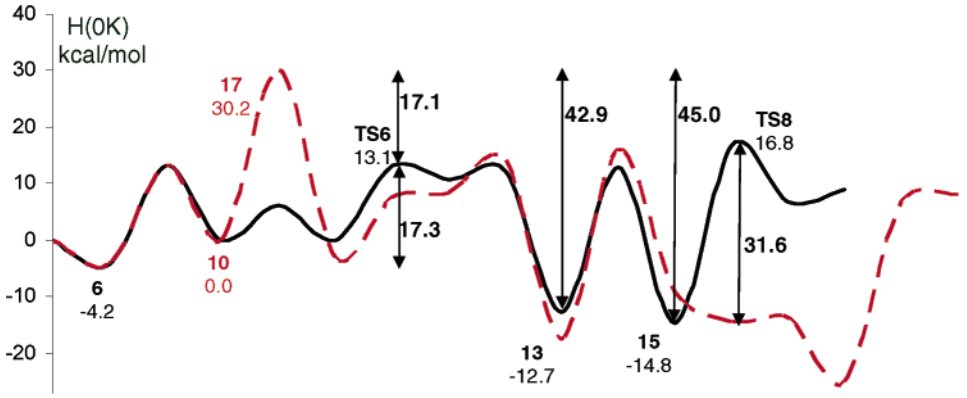

Figure 13. Comparison of ΔH surfaces for C−H activation (solid black line) and Cossee−Arlman (dashed red line) mechanisms.

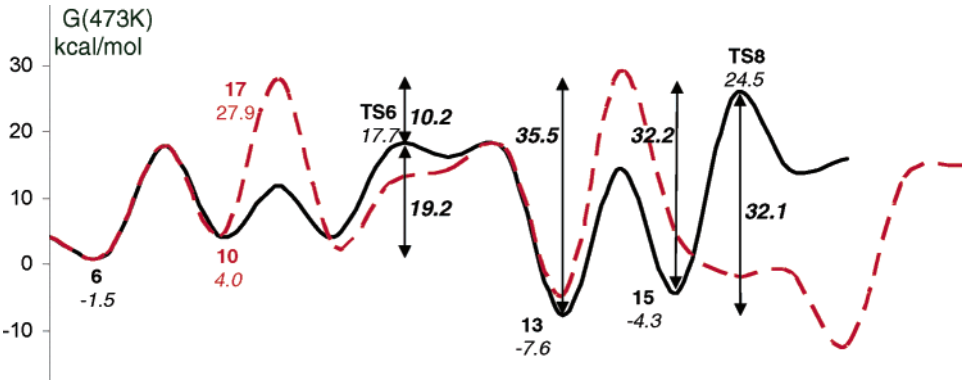

Figure 14. Comparison of ΔG surfaces for C−H activation (solid black line) and Cossee−Arlman (dashed red line) mechanisms.

is not enough to make the Cossee−Arlman mechanism competitive, however, as outlined below.

Other changes between the ΔH and ΔG surfaces includes a change in resting states for the catalyst from **15** on the ΔH surface (−7.6 kcal/mol) to **13** on the ΔG surface (−4.3 kcal/mol). The energy difference between these two states is well within the margin of error, however.

4. Discussion

From the mechanisms in Figures 5−10, it appears that the rate-determining steps for the three potential mechanisms are **8** → **TS3** → **9** ($\Delta H^{\ddagger}$ = 28.8 kcal/mol, $\Delta G^{\ddagger}$ = 28.8 kcal/mol), **13/15** → **TS8** → **16** ($\Delta H^{\ddagger}$ = 31.6 kcal/mol, $\Delta G^{\ddagger}$ = 32.1 kcal/mol), and **10** → **17** + butadiene (ΔH = 34.4 kcal/mol, ΔG = 29.4 kcal/mol). On this basis, we would expect that the pathway through **TS3** (i.e., the one leading to 1-butene) would be the favored mechanism on both the ΔH and ΔG surfaces. However, this is not an accurate comparison, as during the catalytic cycle new resting states are introduced. It should be noted that since **13** and **15** change their relative order when comparing the ΔH and ΔG surfaces, the numbers here consistently assume the lowest of the two (**13** for ΔH and **15** for ΔG).

By overlaying the middle part of the two mechanisms for C−H activation (i.e., the mechanisms after the insertion) in Figure 12, it can be observed that after intermediate **6** the immediate barrier to the 1-butene C−H activation mechanism is **6** → **7**, with a ΔH = 26.5 kcal/mol (ΔG = 21.8 kcal/mol). However, even though the absolute energy of **TS3** is lower than the energy of **7**, this is still the rate-determining step, as **8** → **TS3** has a barrier of $\Delta H^{\ddagger}$ = 28.8 kcal/mol ($\Delta G^{\ddagger}$ = 28.8 kcal/mol) due to the low energy of **8**.

When looking at the mechanism for the production of 2-butene, one can readily observe that the rate-determining step, **13/15** → **TS8**, has a higher absolute barrier than **8** → **TS3**,

$\Delta H^{\ddagger} = 31.6$ kcal/mol ($\Delta G^{\ddagger} = 32.1$ kcal/mol). However, the barrier from **6** → **13/15** through **TS6** is only $\Delta H^{\ddagger} = 17.3$ kcal/mol ($\Delta G^{\ddagger} = 16.2$ kcal/mo1) and should thus be significantly faster than **6** → **7**. The new resting state for the system thus becomes **13/15**, and all barriers must be made relative to the energy of **13/15**. As **13/15** is 8.5 kcal/mol ($\Delta G = 9.1$ kcal/mol) lower in energy than **6**, the *effective* barrier for formation of 1-butene is 36.5 kcal/mol ($\Delta G = 38.9$ kcal/mol), i.e., significantly higher than the barrier for production of 2-butene through **13/15** → **TS8**. Consequently, no 1-butene should be formed initially, and the presence of 1-butene in the final product mixture is instead attributed to isomerization of 2-butene, most likely through an allyl intermediate. This assumption is strengthened by the known isomerization of 1-hexene/2-hexene, which is ~100 times faster than hydroarylation.[25]

Similarly, the Cossee−Arlman mechanism has a barrier of 34.4 kcal/mol ($\Delta G = 29.4$ kcal/mol) from **6**, but an *effective* barrier for **13/15** → **17** of $\Delta H = 45.0$ kcal/mol ($\Delta G = 35.5$ kcal/mol), significantly higher than the barrier for **13/15** → **TS8** (see Figures 13 and 14). The key comparison thus becomes between the rates of butadiene liberation through **17** and conversion to the allyl intermediate through **TS6**. As the difference is $\Delta H = 17.1$ kcal/mol ($\Delta G = 10.2$ kcal/mol), this should be large enough to ensure that all catalyst is converted to **13** or **15** before any butadiene is liberated.

Thus, this catalytic system appears to be the first that dimerizes olefins through a C−H activation pathway. It is very likely this is due to the previously discussed balance between facile [1,2]-insertion and C−H activation,[11] where it appears that factors facilitating insertion debilitates C−H activation, and vice versa. Consequently, a system with lower barriers for insertion would either become a polymerization catalyst or dimerize/oligomerize through the Cossee−Arlman mechanism, while a system with lower barriers for C−H activation would not catalyze the insertion.

It can also be observed that the C−H activation step **TS8** is slightly higher in energy than the insertion transition state, **TS2**, and would thus be the rate-determining step.

(25) Matsumoto, T.; Yoshida, H. *Catal. Lett.* **2001**, *72*, 107.

5. Summary

In summary, we demonstrate that our previously reported C_2H_3-Ir(III)(acac-*O*,*O*)$_2$(Py) system dimerizes olefins through a C−H activation mechanism. The starting catalyst first isomerizes to the cis conformer through a dissociative process, where pyridine is lost, and then adds the olefin substrate to the cis conformer. [1,2]-Insertion of the vinyl moiety into the coordinating olefin generates a Ir−CH_2−CH_2−CH═CH_2 complex, which then isomerizes to an Ir(η^3-allyl) complex through a series of β-hydride transfer reactions. The allyl complex is significantly more stable than any other part of the surface and is expected to be the resting state of the catalyst.

Addition of a second olefin to the allyl complex leads to an Ir−(CH_2−CH═CH−CH_3) complex with a coordinating olefin, which can transfer a hydrogen to generate the product, 2-butene, via a C−H activation transition state. This transition state is the rate-determining step, with a calculated $\Delta H^{\ddagger} = 31.6$ kcal/mol and $\Delta G^{\ddagger} = 32.1$ kcal/mol. This is consistent with the experimentally determined rate of reaction (TOF $\approx 10 \times 10^{-3}$ mol/s).

Other pathways have been explored, most notably the C−H activation pathway to yield 1-butene and the Cossee−Arlman dimerization pathway, initiated by the generation of butadiene. Although both mechanisms have reasonable barriers, they were found to be not competitive due to very facile barriers leading to the η^3-allyl complex. From the η^3-allyl complex, neither 1-butene or butadiene are feasible products. The experimentally observed generation of 1-butene is suggested to occur through isomerization of 2-butene and not through initial formation.

Acknowledgment. The authors thank the National Science Foundation (CHE-0328121) and Chevron-Texaco Energy Research & Technology Company for financial support for this research. We also thank Dr. Robert Nielsen and Mr. John A Keith for valuable discussions regarding thermodynamics in solution.

OM050890X